In situ structural studies of *Anabaena* Sensory Rhodopsin in the *E. coli* Membrane

Meaghan E. Ward[1,2], Shenlin Wang[1,2,$], Rachel Munro[1,2], Emily Ritz[1], Ivan Hung[3], Peter L. Gor'kov[3], Yunjiang Jiang,[4] Hongjun Liang[4], Leonid S. Brown[1,2], Vladimir Ladizhansky[1,2]

[1]Department of Physics and [2]Biophysics Interdepartmental Group, University of Guelph, Guelph, ON, Canada, N1G 2W1.
[3]National High Magnetic Field Laboratory, Florida State University, Tallahassee, FL 32310, United States.
[4]Department of Metallurgical and Materials Engineering, Colorado School of Mines, Golden, Colorado 80401, United States.
[$] Current address: Beijing NMR Center, Peking University, Beijing, China

SUPPORTING INFORMATION

Solid-state NMR spectroscopy

In **Figure S1** we show the pulse sequences used to record data. For both spectrometers, the ^{1}H/X (where X is ^{15}N or ^{13}C) cross-polarization (CP) (1) contact times were 2 ms, with a constant radio frequency (rf) field of 35 and 50 kHz on nitrogen and carbon, respectively, while the proton lock field was ramped linearly around the n = 1 Hartmann/Hahn condition (2). ^{15}N/^{13}Ca and ^{15}N/^{13}CO band-selective transfers (3) were implemented with a contact time of 6 ms. For the ^{13}CA/^{15}N CP, a constant lock field of $2.5\times\nu_r$ ($\nu_r = \omega_r/2\pi$, spinning frequency) strength was applied on ^{15}N, while the ^{13}C field was ramped linearly (10-12% ramp) around $1.5\times\nu_r$. For the ^{13}CO/^{15}N transfer, a constant lock field of $3.5\times\nu_r$ field strength was applied on ^{13}C, while the ^{15}N field was ramped linearly (10% ramp) around $2.5\times\nu_r$. DREAM (4) recoupling with tangential sweep around HORROR (5) recoupling condition was used to accomplish band-selective carbon-carbon polarization transfer in the NCACB experiment. CW proton decoupling at 100 kHz was used during^{15}N/^{13}C CP and DREAM (4). SPINAL64 (6) decoupling optimized around 83 kHz was used during ^{15}N and ^{13}C direct and indirect chemical shift evolutions.

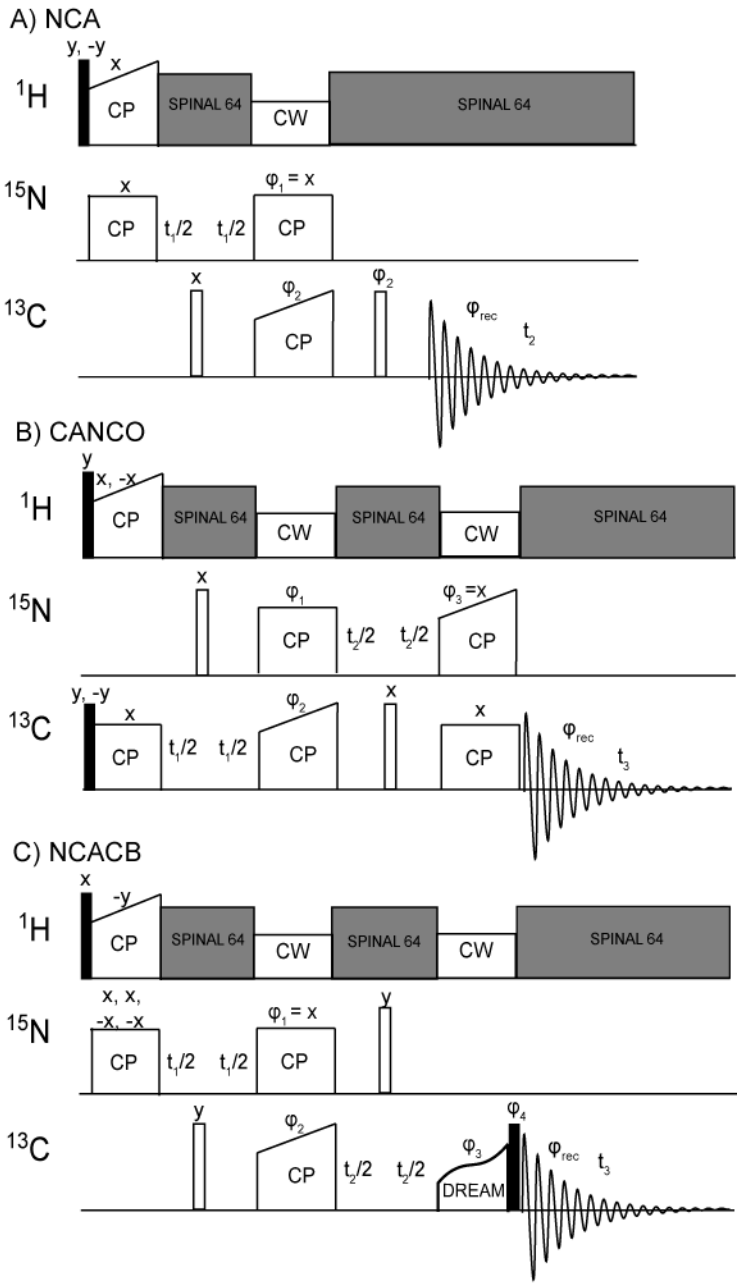

Figure S1. Pulse sequences for **A)** NCA **B)** CANCO and **C)** NCACB experiments. Filled and hollow bars represent $\pi/2$ and π pulses, respectively. In panel **A)**, the following phase cycling was used: φ_2 =(x, x, y, y, -x, -x, -y, -y) and φ_{rec}=(x, x, y, y, -x, -x, -y, -y) and phase sensitive detection is obtained in the indirect t_1 dimension by incrementing φ_1 by 90°. In panel **B)**, the following phase cycling was used: φ_1= (x, x, x, x, -x, -x, -x, -x), φ_2=(x, x, -x, -x), and φ_{rec}=(x, -x, -x, x, -x, x, x, -x) and phase sensitive detection is obtained in the indirect t_1 and t_2 dimensions by incrementing φ_2 and φ_3, respectively, by 90°. In panel **C)**, the following phase cycling was used: φ_2 = φ_3 = (x, x, x, x, -x, -x, -x, -x), φ_4=(x, -x, x, -x) and φ_{rec}=(x, x, -x, -x, -x, -x, x, x) and phase sensitive detection is obtained in the indirect t_1 and t_2 dimensions by incrementing φ_1 and φ_2, respectively, by 90°.

Sample Characterization

In **Figure S2** we show SDS/PAGE analysis of ASR samples in the *E. coli* membrane and proteoliposome environment. We show gels stained with Sypro Ruby Protein stain, which displays all proteins in the sample, as well as Invision His_6-tag stain, which selectively stains proteins, like recombinant ASR, which contain a His_6-tag. To confirm the identity of the high abundance proteins in the ~37 kDa band, the gel band from the EM-ASR lane was subjected to cysteine reduction and carbamidomethylation, followed by trypsin digestion. The extracted peptides were analyzed by an Agilent UHD 6530 Q-TOF Mass spectrometer. Using Peaks 7 software (Bioinformatics Solutions Inc.) the predominant proteins in this band were identified as OmpF and OmpA, with 27 peptides which matched OmpF from *E. coli* and covered 58% of the OmpF sequence and 20 peptides which matched OmpA from *E. coli* and covered 53% of the OmpA sequence, being identified. Therefore the band at ~37 kDa is most likely due to OmpF and OmpA, which likely come from the residual outer membrane fraction.

As the gel is crowded and does not give information on the isotopic labelling of proteins, we use a combination of FTIR and 1D ^{15}N NMR to further analyze the compositions of our samples. Through comparing the integrated area of the Amide I band to the lipid-ester band in FTIR spectra of samples we can determine the protein to lipid ratio. To determine the differing amounts of labelled protein in our UN/UCN as compared to our rbUN/rbUCN samples, we compare 1D ^{15}N spectra. As we show in **Fig. 2B**, we see a reduction in signal in the rbUN EM-ASR sample of about 55% when compared to the UN EM-ASR sample. As the UN and the rbUN EM-ASR samples were isolated in the same way, the protein content of these cells is identical, with only the isotopic labelling of the samples being different. From these two spectra we can estimate that ~45% of the total protein in our rbUN EM-ASR sample is isotopically labelled. Through comparing this spectrum to the PL-ASR spectrum and normalizing for the intensity of selected resolved peaks (**Fig. 2C**) we find that ASR comprises ~1/4 of the total labelled protein content. Therefore, we estimate the relative amount of ASR in the EM-ASR samples to be ~10%.

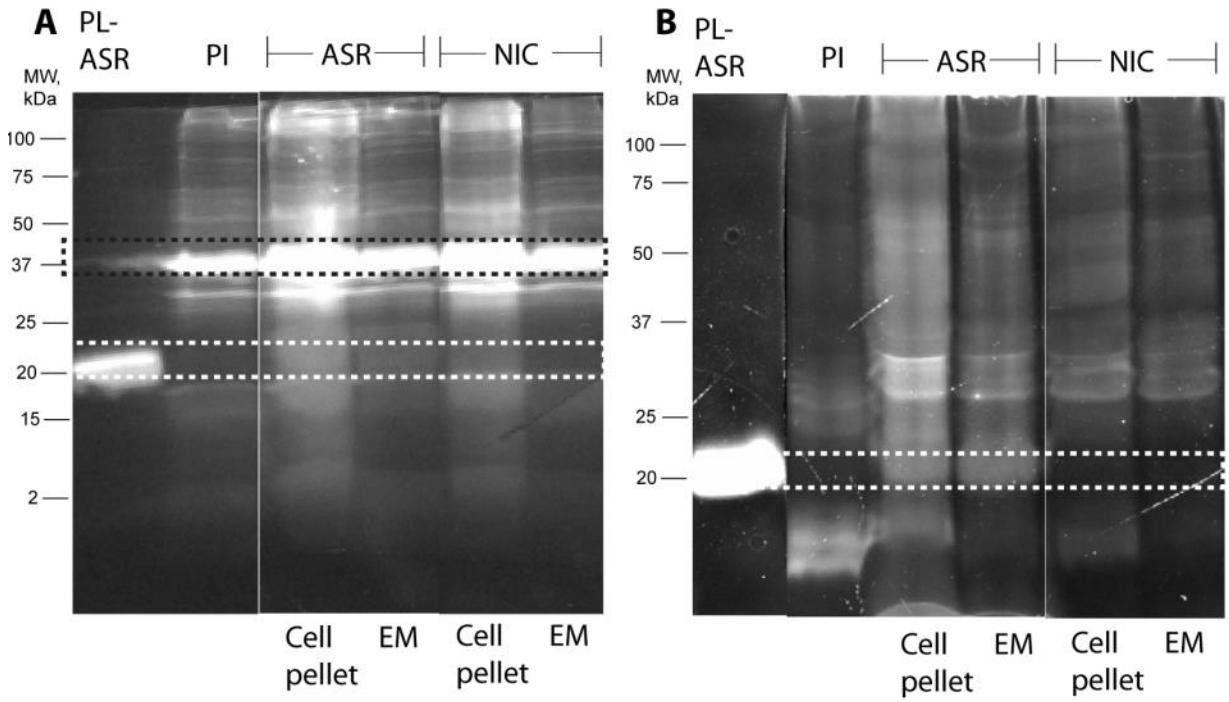

Figure S2. A) Sypro Ruby Protein and **B**) Invision His_6-tag stained SDS/PAGE analysis of *E. coli* membranes from BL21-Codon-plus-RIL cells containing the plasmid for ASR which have been induced (ASR) and not induced (NIC). Samples were taken pre-induction (PI) as well as before (cell pellet) and after EM purification. Membranes were boiled in SDS before electrophoresis. The positions of PL-ASR and the high abundance 37 kDa proteins are indicated with white and black dashed boxes respectively.

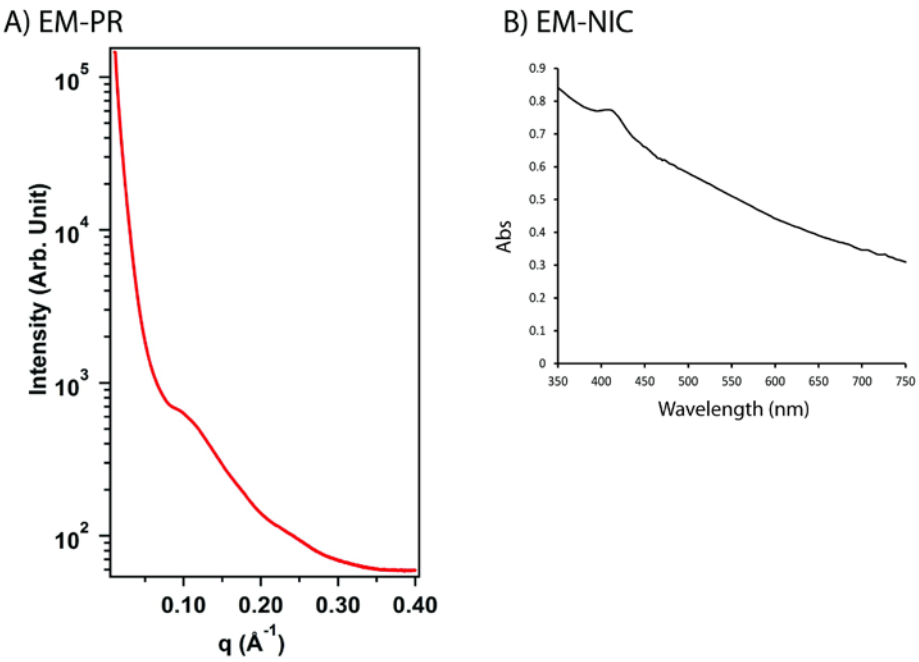

Figure S3. A) Small angle x-ray scattering of green proteorhodopsin (PR) in the *E. coli* membrane. This sample was prepared by applying the protocol used to create the EM-ASR and EM-NIC samples to cells grown in the same *E. coli* strain as our ASR samples, with the expression optimized for PR. The lack of distinct scattering peaks indicates that peaks seen in the EM-ASR spectra are due to the presence of ASR in the sample. B) Absorption spectra of EM-NIC. Though the same scattering and absorption backgrounds as observed in the EM-ASR sample are present, there is no discernible peak at ~540 nm, indicating that the absorption at this wavelength in EM-ASR is due to the presence of ASR.

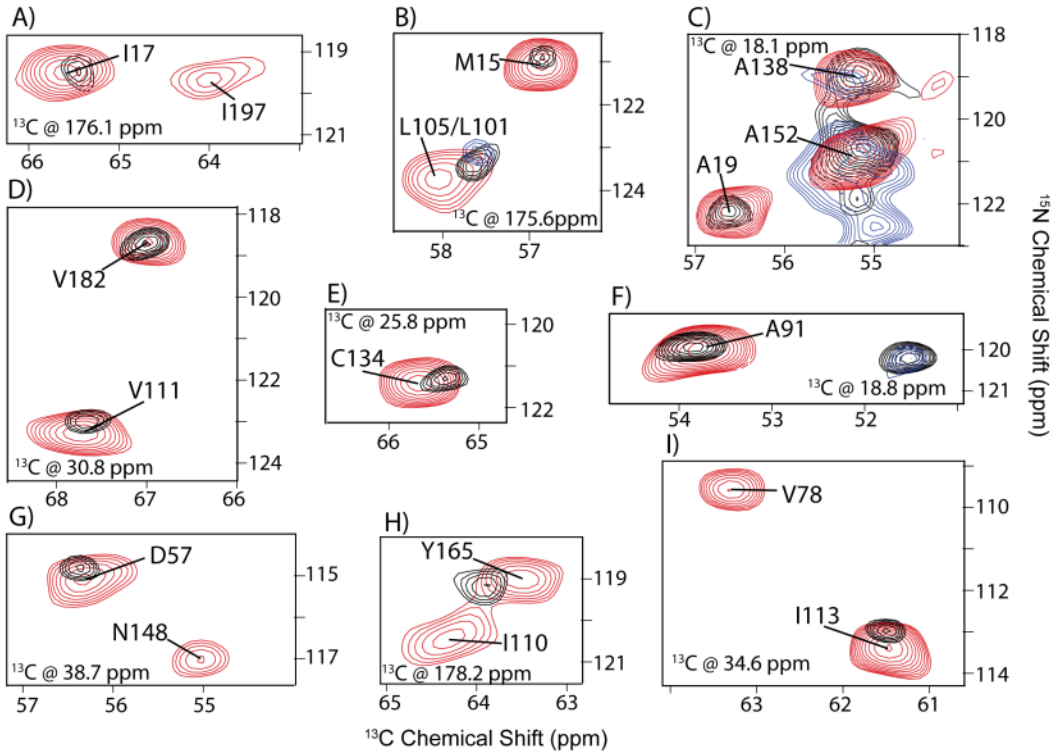

Figure S4. Additional overlaid representative 2D planes of 3D CANCO (A, B, H) and NCACB (C-G, I) experiments performed on PL-ASR (red), EM-ASR (black), and EM-NIC (blue). All peaks are labelled according to the assignments. PL-ASR and EM-NIC spectra were recorded at 800 MHz, while EM-ASR spectra were recorded on a 900 MHz spectrometer. In many cases, peaks which are observable in the PL-ASR spectra are not observed in the EM-ASR spectra due to the reduced sensitivity seen in these spectra. In other cases, ASR peaks cannot be identified in the EM-ASR spectra due to spectral overlap.

Table S1: Summary of chemical shifts in EM-ASR (BMRB entry 25290) and PL-ASR

Residue		EM-ASR Chemical Shift (ppm)				PL-ASR Chemical Shift (ppm)			
		N	CA	CB	C'	N	CA	CB	C'
L	6	116.28	57.17	42.53	176.94	117.27	57.36	42.86	176.79
L	7	117.46	58.85			117.40	58.57		
V	12	121.20	67.84	31.77		121.72	67.91	31.82	
G	14				175.56				175.57
M	15	120.95	56.78	33.62		121.17	56.81	33.58	
T	16				176.12				176.06
I	17	119.29	65.41	37.91		119.54	65.50	38.07	
A	19	122.14	56.59	18.13		122.42	56.54	18.11	
N	28	115.41	50.90		173.48	115.61	50.92		173.45
P	29	130.22	65.12			130.65	65.02		
V	32	125.54	59.63	32.20		125.24	59.82	32.55	
E	36				179.25				179.21
Y	37	115.32	63.40			115.76	63.52		
L	38	121.55	58.93	41.61		121.13	59.00	41.53	
A	40				177.87				177.88
M	41	111.90	59.18			111.11	59.11		
I	43	114.92	67.73		174.40	115.20	67.81		174.72
P	44	132.00	65.34			132.29	65.45		
W	46				176.81				176.97
S	47	106.13	60.01	65.57		106.59	60.11	65.61	
G	48				174.92				174.91
L	49	121.39	58.25			121.63	58.36		
M	52	126.15	59.02	33.13	177.51	126.24	59.13	33.04	177.45
A	53	118.45	54.71	17.76	179.19	118.52	54.74	17.39	179.21
M	54	113.21	58.55	31.22		114.04	58.67	31.16	
A	55	126.94	55.53	15.61	179.19	127.23	55.49	15.57	179.39
I	56	111.09	60.48			111.05	60.46		
D	57	114.75	56.35	38.72	174.76	115.57	56.37	38.66	174.97
Q	58	117.66	54.54	32.08		117.62	54.74	32.25	
G	59	101.78	45.83			101.86	45.97		
K	60	114.05	53.77	36.44		114.34	53.85	36.55	
V	61	120.15	59.98	35.71		120.67	59.94	35.77	
A	63	128.93	52.25	21.39		128.99	52.21	21.57	
Q	66				172.43				172.42
I	67	119.16	58.96	35.95		119.34	59.22	36.25	
A	68	134.28	50.80			134.16	50.92		
A	71	124.83	55.18	17.33		125.12	55.25	17.20	
Y	73	112.76	59.87	38.04	177.33	112.81	59.71	37.89	177.27

I	74	119.97	65.66			119.99	65.99		
D	75	116.04	56.00	40.87		116.21	55.96	40.92	
W	76	114.87	56.59	29.93		114.92	56.54	29.94	
M	77				172.92				172.72
V	78	109.88	63.25	34.35	178.75	109.73	63.34	34.37	178.67
T	79	107.37	66.03			107.43	66.14		
T	80	113.05	67.06			112.93	66.93		
L	82	113.70	57.52	41.30		113.75	57.60	41.10	
A	91	119.91	53.89	18.81		120.20	53.73	18.84	
M	92	109.43	53.53			109.65	53.31		
K	96	119.32	56.59	32.88		119.73	56.54	32.55	
T	101				178.51				178.30
I	102	117.16	66.53	38.16		117.26	66.46	38.19	
M	106	113.70	61.16	35.09		114.10	61.23	35.16	
Q	109	121.43	57.17	26.67		122.19	57.25	26.67	
V	111	123.07	67.72	30.85		123.48	67.79	30.73	
V	112	121.08	67.13	31.71		121.86	67.40	31.73	
I	113	113.00	61.51	34.60		113.63	61.47	34.61	
S	115	115.57	63.62	62.44		116.56	63.81	62.34	
L	117	123.19	57.17	40.87		123.48	57.25	40.92	
A	119	122.49	56.12	19.36		123.01	56.07	19.51	
D	120	113.00	54.13	40.31		113.05	54.08	40.68	
S	122	115.57	61.63	63.85		115.39	61.58	63.79	
V	127	122.25	65.84	31.65		122.42	65.68	31.64	
W	131	119.56	61.11	29.25		119.61	61.35	29.34	
C	134	121.32	65.40	25.81		121.60	65.68	25.88	
G	135				175.99				176.00
V	136	123.35	67.43	31.28		123.76	67.58	31.22	
C	137	118.62	65.49	26.86		118.79	65.80	26.79	
G	145				175.55				175.51
I	146	114.64	64.26	35.62	178.20	114.86	64.38	35.52	178.30
W	147	120.89	60.03	30.05		120.86	60.01	30.06	
T	154	107.15	63.79			106.90	63.78		
T	156	104.50	61.51			104.87	61.44		
S	158	113.00	57.88	65.20		113.40	57.72	65.31	
S	159	118.50	61.51	62.74		118.32	61.58	62.82	
A	162	122.96	56.00	17.82		123.53	56.07	18.02	
L	164				178.20				178.12
Y	165	119.29	63.94			119.04	63.52		
D	166	119.21	56.94	39.33		119.14	56.78	39.53	
V	169	120.38	64.67	29.93		119.85	64.51	29.94	
Y	171				175.32				175.39
F	172	118.33	60.72			118.08	60.83		

T	173	113.13	68.94			113.01	68.96		
L	175				179.75				179.64
W	176	117.71	62.65			117.67	62.66		
G	178	102.39	47.59			102.23	47.49		
I	181				175.69				175.45
V	182	118.74	66.98	30.73		118.90	67.02	30.67	
W	183	116.40	62.68	32.39		116.56	62.75	32.25	
I	184	113.35	61.04	39.58		113.28	60.76	39.47	
G	186				174.02				173.81
P	187	133.53	64.85			133.66	64.91		
I	193	107.11	58.56		175.28	106.66	58.44		175.03
N	194	118.32	51.35			118.49	51.37		
Q	195	115.81	57.76	29.25		116.33	57.60	29.28	
F	200	120.38	61.98	38.96		120.43	61.93	38.98	
L	201				178.39				178.54
F	202	115.48	60.76	35.83		115.37	60.74	35.64	
C	203	117.92	62.33	28.64		117.85	62.52	28.61	
G	212				173.54				173.27
F	213	119.83	62.44			119.86	62.12		

Supporting References

1. Pines, A., M.G. Gibby, and J.S. Waugh. 1973. Proton-enhanced NMR of dilute spins in solids. J. Chem. Phys. 59: 569–590.

2. Hartmann, S.R., and E.L. Hahn. 1962. Nuclear double resonanace in the rotating frame. Phys. Rev. 128: 2042–2053.

3. Baldus, M., A.T. Petkova, J. Herzfeld, and R.G. Griffin. 1998. Cross polarization in the tilted frame: assignment and spectral simplification in heteronuclear spin systems. Mol. Phys. 95: 1197–1207.

4. Verel, R., M. Ernst, and B.H. Meier. 2001. Adiabatic dipolar recoupling in solid-state NMR: the DREAM scheme. J. Magn. Reson. 150: 81–99.

5. Hohwy, M., H.J. Jakobsen, M. Eden, M.H. Levitt, and N.C. Nielsen. 1998. Broadband dipolar recoupling in the nuclear magnetic resonance of rotating solids: a compensated C7 pulse sequence. J. Chem. Phys. 108: 2686–2694.

6. Fung, B.M., A.K. Khitrin, and K. Ermolaev. 2000. An improved broadband decoupling sequence for liquid crystals and solids. J. Magn. Reson. 142: 97–101.